Mäkelä, Eveliina; Escobedo, José Luis González; Lindblad, Marina; Käldström, Mats; Meriö-Talvio, Heidi; Jiang, Hua; Puurunen, Riikka L.; Karinen, Reetta

Hydrodeoxygenation of levulinic acid dimers on a zirconia-supported ruthenium catalyst

Published in:
Catalysts

DOI:
10.3390/catal10020200

Published: 01/02/2020

Document Version
Publisher's PDF, also known as Version of record

catalysts

MDPI

Article

Hydrodeoxygenation of Levulinic Acid Dimers on a Zirconia-Supported Ruthenium Catalyst

Eveliina Mäkelä [1,*], José Luis González Escobedo [1], Marina Lindblad [2], Mats Käldström [2,†], Heidi Meriö-Talvio [1], Hua Jiang [3], Riikka L. Puurunen [1] and Reetta Karinen [1]

[1] Department of Chemical and Metallurgical Engineering, Aalto University School of Chemical Engineering, P.O. Box 16100, 00076 AALTO, Finland; jose.gonzalezescobedo@aalto.fi (J.L.G.E.); heidi.merio-talvio@aalto.fi (H.M.-T.); riikka.puurunen@aalto.fi (R.L.P.); reetta.karinen@aalto.fi (R.K.)

[2] Neste Corporation, P.O. Box 310, 06101 Porvoo, Finland; marina.lindblad@neste.com (M.L.); makaldst@abo.fi (M.K.)

[3] Department of Applied Physics, Aalto University School of Science, P.O. Box 15100, 00076 AALTO, Finland; hua.jiang@aalto.fi

* Correspondence: eveliina.makela@aalto.fi

† Present address: Walki Group, P.O. Box 121, 68601 Pietarsaari, Finland

Received: 18 December 2019; Accepted: 1 February 2020; Published: 7 February 2020

Abstract: The hydrodeoxygenation (HDO) of levulinic acid (LA) aldol condensation product dimers was studied between 250 and 300 °C and 50 bar H_2 in a batch reactor with Ru catalyst supported on mesoporous zirconia. During the reaction, the unsaturated dimers, which contained ketone groups and double bonds, were hydrogenated to saturated dimers. A greater degree of deoxygenation was achieved at higher temperatures, and oxygen was removed as water and CO_2. Oxygen removal was evidenced by elemental analysis and infrared spectroscopy, in which the C=O peak decreased with increasing temperature. A drawback of high reaction temperature (300 °C) was a minor degree of oligomerization. The formation of aromatics was also observed at the higher temperatures. Aside from the saturated dimers, volatile products were obtained at all temperatures, including ketones, acids, and esters. This study demonstrates for the first time the potential of LA dimers as a sustainable route from lignocellulosic biomass to biofuels and biocomponents.

Keywords: levulinic acid; dimer; hydrodeoxygenation; ruthenium; zirconia

1. Introduction

Climate change, the growing global energy demand, and the concerns related to insufficient reserves of fossil-based products have prompted the booming research in bio-based fuels and chemicals. A recent review by Oh et al. [1] discusses the main barriers for biorefining including a shortage of raw material, as over 90% of the total biofuels are currently produced from edible biomass. One option to replace fossil fuels and chemicals is lignocellulose, which is considered as the main source of cheap and abundant non-edible plant-based biomass [2].

Various platform chemicals can be obtained from lignocellulose, such as levulinic acid (LA) and furfural [3], but carbohydrate-based chemicals have only five or six carbons depending on the parent monosaccharide [4]. In order to produce, e.g., bio-based jet fuel or diesel, extended carbon chains ($>C_6$), which could be further deoxygenated to alkanes, have received attention [5,6]. Various ways to increase the carbon chain length of the lignocellulosic platform chemicals exist: aldol condensation, ketonization, and alkene oligomerization [7]. These reactions lead to heavier compounds, for example dimer or trimer structures [7].

Several authors have studied the reactions to increase carbon chain length. The Dumesic research group has studied aldol condensation between furfural or 5-(hydroxymethyl)furfural (HMF) and acetone and aldol self-condensation of hydrogenated HMF [8,9]. The coupling of these molecules has been also reported using an organocatalytic approach [10,11]. Li et al. [12] and Corma et al. [13] produced diesel fuel from further processing the hydroxyalkylation–alkylation (HAA) product of 2-methylfuran. The Dumesic research group has also studied the ketonization of γ-valerolactone (GVL) via intermediate ring-opening to pentanoic acid to form 5-nonanone [14,15] and the oligomerization of butenes produced from GVL through pentenoic acid [16]. Recently, Mascal et al. [5] presented the hydrodeoxygenation (HDO) of Angelica lactone dimer (through levulinic acid intramolecular dehydration and further oligomerization to dimers) in order to produce C_7–C_{10} hydrocarbons. Finally, the formation of oxo-carboxypentyl-γ-valerolactone during LA hydrodeoxygenation via LA dimerization through aldol addition and dehydrative cyclization was reported by Grilc et al. [17].

The structure and production of LA dimers through aldol condensation was first described by Blessing and Petrus [18]. Recently, the production of LA dimers has been described by several authors using hydrogenating conditions with a Pd containing ion-exchange resin as a catalyst, basic MgZr oxide catalysts in water, or $ZnCl_2$ catalyst in trichloroacetic acid [7,19–21]. The formation of LA dimers in hydrogenating conditions and the mixture of identified LA dimers in the feed used in this work are presented in Scheme 1. The LA dimers have potential applications, upon further processing, as fuel additives, surfactants, plasticizers, hydraulic fluids, and lubricants [19,20,22].

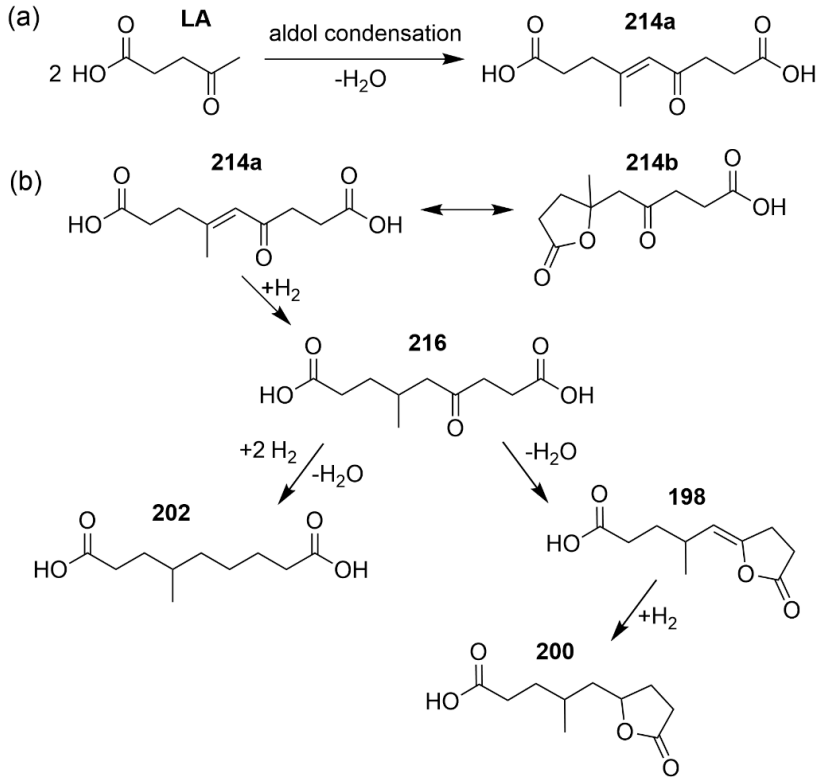

Scheme 1. (**a**) Levulinic acid (LA) dimer formation through aldol condensation, (**b**) identified LA dimers in the feed mixture with corresponding molecular weights and reactions among them.

The potential for HDO upgrading of these dimers was discussed by van den Brink et al. [23]; however, they mainly reported experiments using ethyl levulinate as a model compound. With Ni and noble metal on silica or silica-bound β-zeolite (80 bar H_2, 250 °C, 4 h, 500 rpm), they obtained GVL and ethyl pentanoate and/or pentanoic acid as the main products. With the less acidic support (silica), only GVL was obtained. van den Brink et al. [23] also tested the hydrogenation of LA dimers

diluted in ethanol using Ni and Pt on silica-bound β-zeolite (80 bar H_2, 240 °C, 75 h, 500 rpm) and reported the disappearance of carbonyl groups, although they did not provide any information on the product. Recently, González Escobedo et al. [24] studied the potential of LA dimers using γ-nonalactone (GNL) as a model compound representing the lactone moieties in some of the LA dimers (Scheme 1). From the used noble metal catalysts (Ru, Rh, Pt and Pd supported on ZrO_2), Ru provided the highest selectivity to hydrocarbons, almost 24%, at 280 °C and 60 bar H_2 after 5 h reaction time [24]. To our knowledge, no attempts to upgrade LA dimers by HDO have been reported with a description of the product obtained.

In this study, the HDO of LA dimers was demonstrated for the first time using a Ru catalyst with the aim of determining the feasibility of removing the oxygen and investigating the product distribution. As noble metal catalysts have been reported to have high activity in C–O hydrogenolysis [25,26] and due to the initial HDO study with GNL by González Escobedo et al. [24], Ru was selected as a catalyst in this study. ZrO_2 support was chosen over conventional γ-Al_2O_3 to prevent excess coking and to obtain high water tolerance and thermal stability [26,27].

2. Results and Discussion

2.1. Catalyst Characterization

The weight-based metal content of the prepared catalyst was 3.6% by X-ray fluorescence (XRF), which was also used as a basis for dispersion calculation. The physisorption isotherms and the Barrett–Joyner–Halenda (BJH) pore size distributions for the ZrO_2 support and the Ru/ZrO_2 catalyst are presented in Figure 1a,b, respectively. The specific surface areas of both the support and the Ru catalyst were around 70 $m^2\ g^{-1}$. No significant differences were observed in the pore volume or in the average pore diameter either (Table 1). The Ru dispersion calculated from the H_2 chemisorption measurement was 25%, and the average particle size 3.7 nm. Based on scanning transmission electron microscopy (STEM) analysis of the fresh, thermally treated Ru/ZrO_2 catalyst (Figure 2 and Figures S1–S3 in the Supplementary Materials), the Ru particles appeared to be unevenly distributed on the ZrO_2 support. Although the presence of Ru was unambiguously confirmed with energy-dispersive X-ray spectroscopy (EDS) mapping (Figure 2), it was difficult to estimate the Ru particle size reliably from the images, due to the poor contrast between Ru and Zr in STEM (Figure S2). In Figure S1, Ru was also detected on the ZrO_2 support, but it was difficult to estimate the particle size. Figure 2a shows a relatively large Ru particle of approximately 25 nm in diameter. EDS mapping (Figure 2b–e) demonstrates that Zr (Figure 2c) and O (Figure 2d) elements are evenly distributed throughout the sample, while Ru (Figure 2b) shows a well-defined shape. Figure 2e is an overlay image, which highlights the existence of Ru.

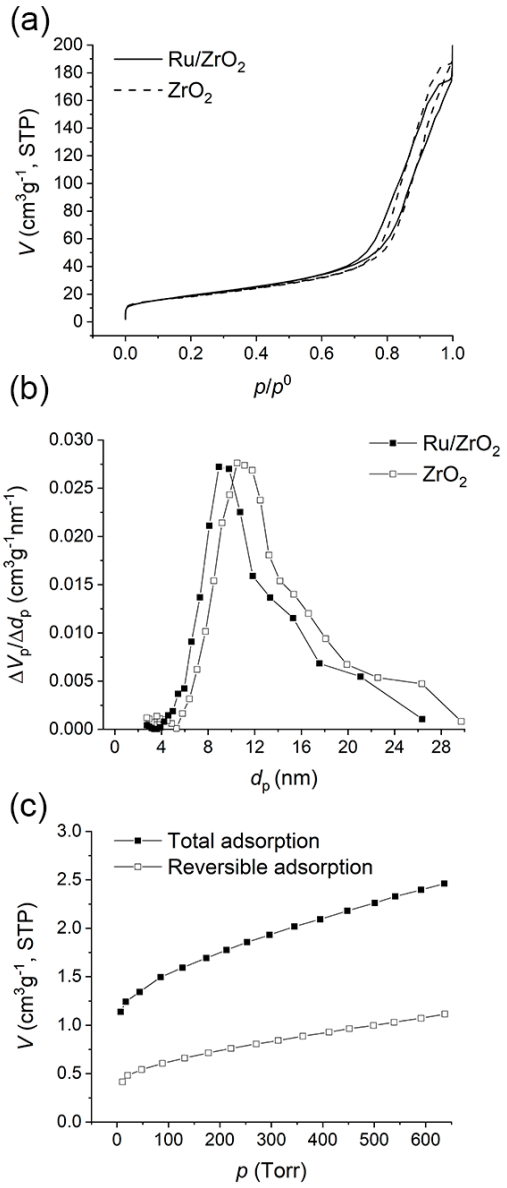

Figure 1. (**a**) Nitrogen physisorption isotherms at −196 °C, (**b**) the Barrett–Joyner–Halenda (BJH) pore size distribution calculated from the desorption branch 0.2–0.9 p/p^0 and (**c**) the total H_2 chemisorption isotherm (■) and the reversible H_2 adsorption isotherm (□) measured at 75 °C.

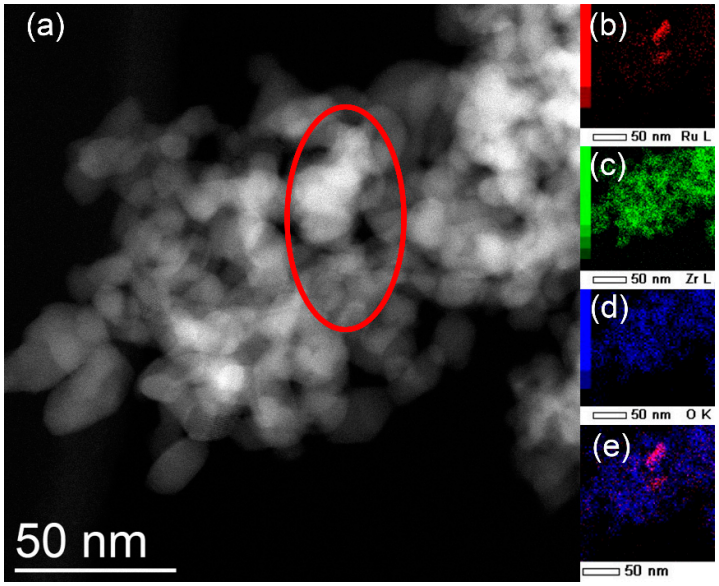

Figure 2. Results of *S*TEM analysis of the fresh, thermally treated Ru/ZrO_2 catalyst: (**a**) STEM dark-field image, (**b**–**e**) energy-dispersive X-ray spectroscopy (EDS) mapping of Ru (**b**), Zr (**c**), O (**d**), and overlay display (**e**). The red ellipse indicates the area where Ru particles were identified in the EDS mapping.

Temperature-programmed reduction (TPR) experiments were performed on the catalyst to mimic the reduction conditions in the HDO reactor (Section 3.5) and to assess the effect of exposing the reduced catalyst to the atmosphere during feed loading. Thus, TPR experiments were performed after reduction and exposure to air, and after reduction without exposure to air (Section 3.3). The TPR profiles of the Ru/ZrO_2 catalyst are presented in Figure 3. The reduction profile of the fresh, thermally treated catalyst (Figure 3, solid lines) revealed a large peak from 100 to 170 °C, both in the thermal conductivity detector (TCD) and in the 2 amu mass spectrometer (MS) signal, which monitored H_2 consumption (Supplementary Materials Figure S4a). In the TPR profiles obtained after reducing the catalyst (dotted lines), there was barely any difference between the catalyst that was exposed to air after reduction (Figure 3a) and the catalyst that was not exposed to air (Figure 3b). The small peak at 100 to 130 °C observed in the TCD signals of the reduced catalysts (Figure 3, dotted lines) appeared also in the 2 amu MS signal. The 18 amu MS signal (H_2O) in the TPR of the fresh, thermally treated catalyst increased up to 100 °C, remained flat up to 350 °C, and fell abruptly at the start of the 350 °C isothermal hold (Figure S4a). In the TPR of the reduced catalyst, the H_2O MS signal rose simultaneously with H_2; the former peaked at 130 °C, and the latter peaked at 105 °C (Figure S4c). Based on the TPR experiments, the in situ reduction of the Ru catalyst in the HDO experimental protocol seems sufficient despite the opening of the reactor after the reduction step to add the LA dimer feed.

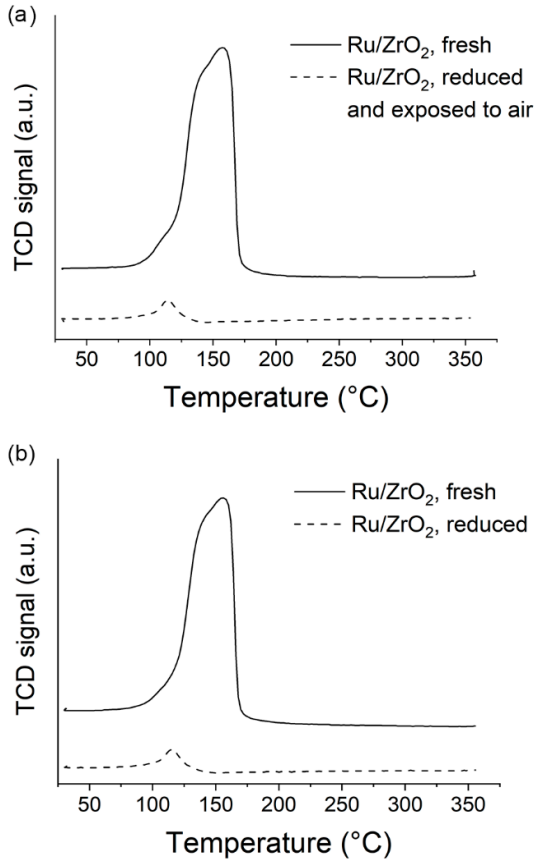

Figure 3. Temperature-programmed reduction (TPR) profiles of Ru/ZrO_2 catalyst before and after reduction at 350 °C for 2 h. (**a**) The catalyst was exposed to air for 20 min after reduction, (**b**) the catalyst was not exposed to air.

Thermogravimetric analysis (TGA) was performed on the spent Ru/ZrO_2 catalysts to obtain the amounts of solids deposited on the catalysts during HDO. Examples of the TGA of a HDO liquid product and of the corresponding spent catalyst are presented in Figure 4. In the TGA of the dimer feed and the HDO experiment products, 98% to 99% of the liquid mass was lost during the evaporation step in N_2, regardless of the amount of material loaded (10 to 18 mg). Most of the evaporation took place between 200 and 300 °C. It is possible that pyrolysis, and not only evaporation, could have occurred during this step, especially in the presence of the catalyst. Nevertheless, for the calculations, it was assumed that the same fraction of liquid was lost with and without the catalyst, for a lack of more details. In the TGA of the soaked, spent catalysts, the combustion (after the evaporation) took place mostly in a sharp step around 250 °C, and a small loop appeared at the end of that step (Figure 4b). The mass gain represented by the loop was removed for the calculation of solid deposits (Equation (7)). The mass ratios of solid deposits (m_s in Equations (5)–(7)) to final dry catalyst ($m_{cat,f}$) were calculated as 0.05, 0.04, 0.05 and 0.04 for spent catalyst used in the HDO experiments at 250 °C, 275 °C, 300 °C and 250 °C (τ_b = 1.1 g_{cat} g_{feed}^{-1} h), respectively. Thus, solid deposition on the catalyst occurred in all the studied HDO conditions.

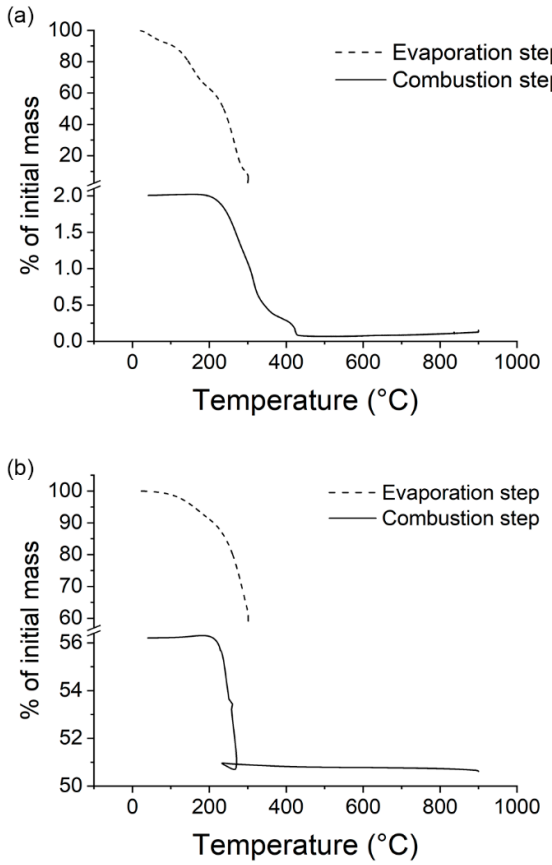

Figure 4. Thermogravimetric analysis (TGA) thermograms of (**a**) the product of experiment at 250 °C, (**b**) the spent Ru/ZrO_2 (250 °C) catalyst soaked in product. Note the scale breaks.

Table 1. Summary of the characterization results from X-ray fluorescence (XRF), physisorption, and chemisorption.

Catalyst	XRF	Physisorption			Chemisorption		
	Metal content	S_{BET} [1] (m^2 g^{-1})	Pore volume [2] (cm^3 g^{-1})	Average pore diameter [2] (nm)	Irreversible adsorption capacity (μmol_{gas} g_{cat}^{-1})	Dispersion	Average particle size (nm)
ZrO_2	-	67	0.18	13	-	-	-
Ru/ZrO_2	3.6%	70	0.21	11	43.9	25	3.7

[1] Calculated via Brunauer–Emmett–Teller (BET) method from 0.05 to 0.3 p/p^0, [2] Calculated via BJH method using desorption data from 0.2 to 0.9 p/p^0.

2.2. Relative Change of LA Dimers

The HDO experiments were conducted in batch reactor system with Ru/ZrO_2 catalyst and thermally. The experiments were carried out at temperatures between 250 and 300 °C with a batch residence time (τ_b) of 0.6 or 1.1 g_{cat} g_{feed}^{-1} h.

The analysis of the dimer mixture (referred to also as feed) with high-performance liquid chromatography (HPLC) revealed six main components with molecular weights of **216** (70 area-%), **214** (10 area-% including both isomers), **202** (4 area-%), **200** (10 area-%), and **198** (6 area-%). In addition to these dimers, various isomers could also have formed during the production of the feed mixture. HPLC total ion current (TIC) chromatograms of the feed and selected products are presented in the Supplementary Materials (Figure S5). In addition, the mixture also contained a small amount of unreacted LA. The relative changes (Equation (2)) of individual dimers are presented in Figure 5. A positive relative change indicates a net increase in the amount during the reaction. Especially the more reactive dimers (**214a**, **214b** and **216**) were converted with relative changes of over −90% not

Bold is not necessary; however, we think that it quite nicely highlights that it is not just a number, but the 'name' of the individual dimer also.only to other products, but also to less reactive dimers, such as dimers **200** and **202** in all the catalytic experiments. The reactions of dimers **214a**, **214b**, and **216** in hydrogenating conditions through HDO and further lactone formation were also observed by Käldström et al. [7]. In addition to dimers **214a**, **214b**, and **216**, dimer **198** was mainly consumed in the catalytic experiments, whereas dimers **200** and **202** were formed. No significant difference was obtained with the higher batch residence time (1.1 g_{cat} g_{feed}^{-1} h). The thermal experiment was not able to fully convert dimers **214a**, **214b**, and **216**, unlike the catalytic experiments, but interestingly, a significant production of dimer **198** was observed.

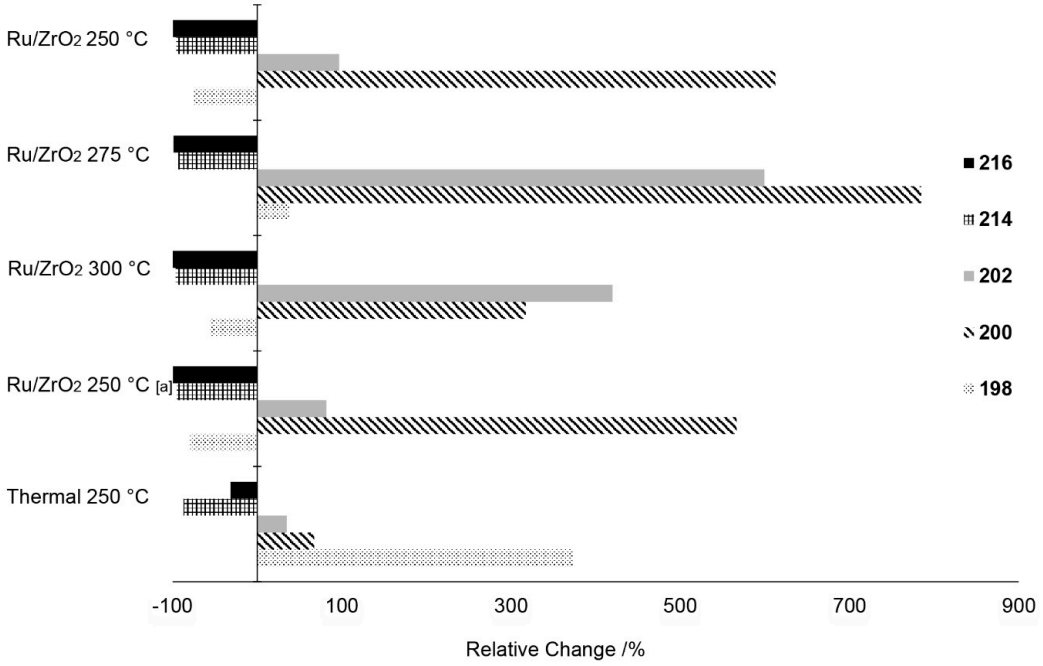

Figure 5. Relative changes of the levulinic acid (LA) dimers obtained with Ru/ZrO_2 catalyst and thermally. Dimer **214** includes both isomers **214a** and **214b** (Scheme 1). [a] τ_b = 1.1 g_{cat} g_{feed}^{-1} h.

2.3. Elemental Composition

The oxygen content of the feed and the products obtained after the catalytic and thermal experiments were studied with elemental analysis. The van Krevelen diagram [28] (Figure 6) revealed that the catalysts and thermal experiments removed some oxygen, but full deoxygenation was not achieved. Moreover, the H/C ratios were also decreasing with respect to the feed in all the experiments, indicating more unsaturation in the obtained organic products, especially at high temperature. Compared to standard diesel, the O/C and H/C ratios remained higher and lower, respectively [29].

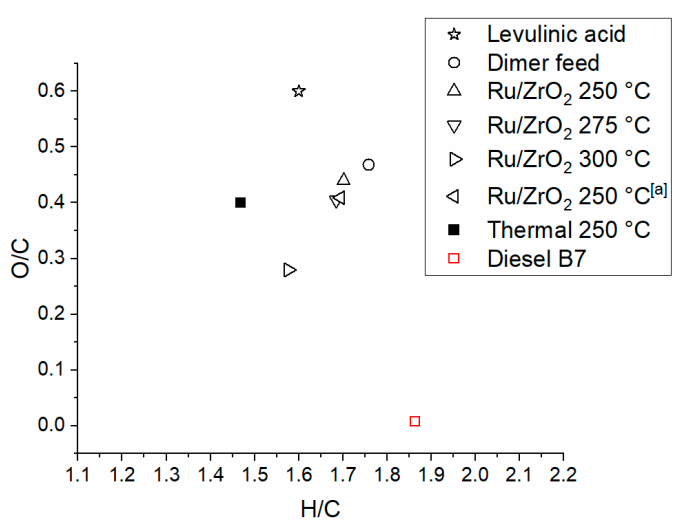

Figure 6. van Krevelen diagram of the molar H/C and O/C ratios of the dimer feed and the organic liquid product mixtures compared to levulinic acid and standard diesel [29]. [a] τ_b = 1.1 g_{cat} h g_{feed}^{-1}.

2.4. Molecular Sizes of the Products

Gel permeation chromatography (GPC) was used to study the molecular sizes of the organic product mixtures with three standard molecules for comparison: stearic acid (SA, 284 amu), azelaic acid (AA, 188 amu), and levulinic acid (LA, 116 amu). Of the standards, only LA was exhibiting UV (270 nm) absorbance due to the C=O chromophore. Figure 7 presents the obtained chromatograms with refractive index (RI) and ultraviolet (UV) detectors.

With the RI detector (Figure 7a,b), the feed presented two main peaks at 9.0 and 9.5 min. The higher peak, with molecular mass close to azelaic acid, decreased in all the experiments, especially in the catalytic ones. This peak likely contained dimer **216**, which was the most abundant in the feed. The second peak attributed to the feed at 9.5 min increased in the experiments, which could be explained by the converting of dimers **214a**, **214b**, and **216** to the less reactive dimers (**200** and **202**) as noticed also from the relative change calculations (Figure 5). The small peak at 10.2 min indicates that also lighter compounds than levulinic acid were present already in the feed, but the amount was increased in the experiments. The light products had at least two major molecular sizes, as two peaks were identified. One peak had similar retention time to levulinic acid and was formed at 300 °C in the catalyzed experiment. Another peak occurred at the retention time of 10.2 min in the thermal experiment and with catalyst, but the shape differed slightly compared to the thermal experiment, which could mean that the compounds causing the peak were different. Heavier compounds (eluting before SA, molecular mass >284 amu) were also formed especially at higher reaction temperatures with the catalyst and thermally.

The UV detector (Figure 7c,d) was used to reveal possible chromophores forming in the reaction. The wavelength of 270 nm is especially suitable for detecting aromatic chromophores and conjugated systems exhibiting medium or strong absorption in UV region [30]. Carbonyl derivatives exhibit only weak absorption between 250 and 350 nm [30]. As the broad peak from 7.0 to 9.5 min was growing with increasing reaction temperature, UV chromophores were formed different to the feed. At low temperature (250 °C), the catalyst resulted in almost no UV absorption whereas at higher temperatures, the products started to absorb UV light. In the thermal experiment, several peaks were obtained in the same positions as in the catalytic experiments (7.0–9.5 min), but there was also a strong peak after retention time of 10 min. In addition, a peak having the same retention time as LA was formed, which was present in some of the catalytic products as well. Since LA should only have a weak UV absorbance at 270 nm and the corresponding peak with the RI detector remained small, it is likely that no LA was produced but rather molecules of similar size but different chemical nature.

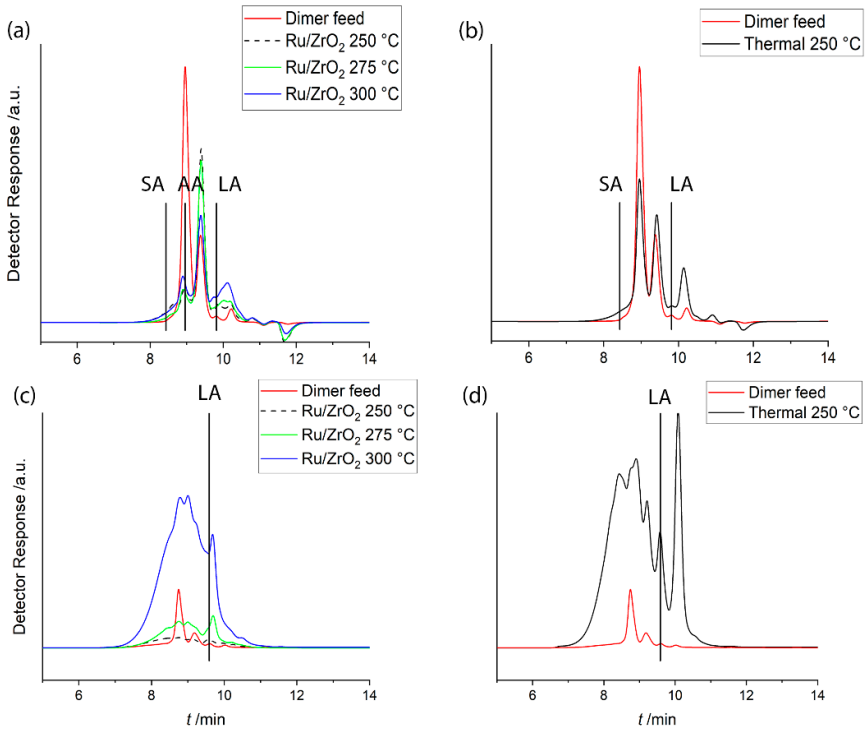

Figure 7. Gel permeation chromatography (GPC) chromatograms of the dimer feed and the products obtained with Ru/ZrO_2 catalyst and thermally at various temperatures. (**a**,**b**) with refractive index (RI) detector (equal scaling), and (**c**,**d**) with UV detector (270 nm, equal scaling). SA: stearic acid (284 amu), AA: azelaic acid (188 amu), LA: levulinic acid (116 amu).

2.5. Product Composition by Infrared Spectroscopy

Infrared (IR) spectra of the dimer feed and the samples obtained with the Ru catalyst and thermally are presented in Figure 8. All the samples were highly complex and contained several functional groups; thus, IR could only be used to indicate the disappearance or appearance of certain functional groups. In the O–H stretching region (Figure 8c,d), the broad band from 3400 cm^{-1} to 2400 cm^{-1}, especially visible with the feed, is attributed to O–H in carboxylic acid [31]. The peak has overlapping with sp^3 C–H stretching, which is visible as a sharper band at ca. 3000–2850 cm^{-1} with three peaks [31]. The O–H stretch band from carboxylic acid decreased slightly in the thermal experiment, but more so with the catalysts, suggesting the consumption of acid groups. Figure 8c,d also contain information of O–H stretching from alcohols or water trapped in the organic product, which is visible both with the catalyzed and the thermal experiments. The band from 3600 to 3300 cm^{-1} is attributed to O–H with H-bonding and the peak at 3650 cm^{-1} (Ru, 300 °C) is attributed to free O–H [31,32]. At high temperature, less oxygen was left in the product (Figure 6); thus, there was less hydrogen bonding between the molecules causing the emerging of the free O–H stretching with Ru at 300 °C.

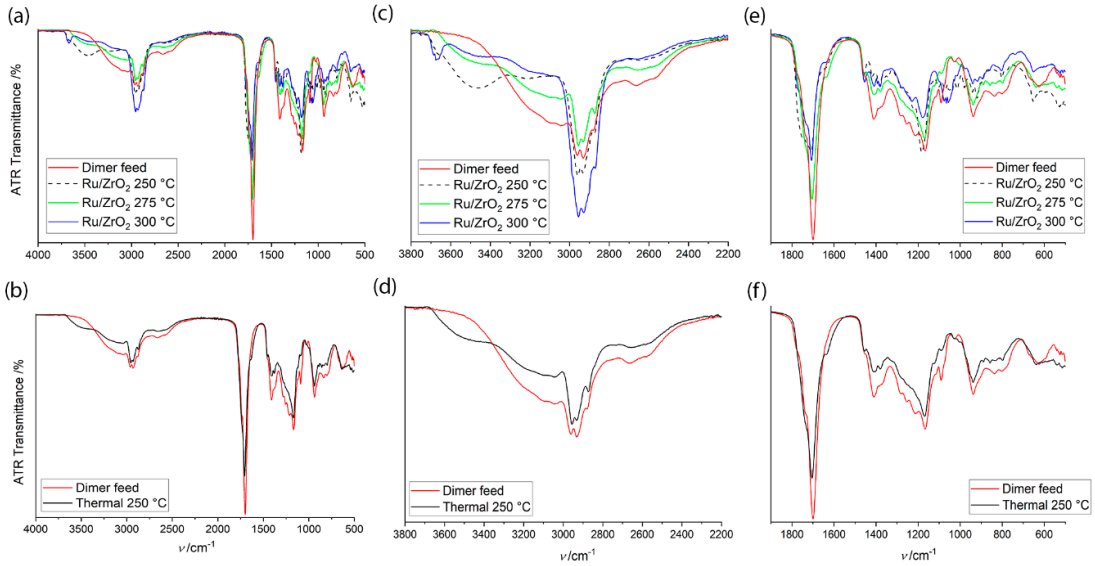

Figure 8. Attenuated total reflection (ATR) IR spectra of the feed and the samples obtained with (**a**) Ru catalyst in different temperatures and (**b**) thermally at 250 °C. (**c**,**d**) O–H and sp^3 C–H stretching range, (**e**,**f**) C=O stretching range and the fingerprint region.

The sharp peak at approximately 1700 cm^{-1} is attributed to C=O bond stretching (Figure 8e,f) [30–32]. In the catalytic experiments, the C=O peak decreased significantly with increasing the reaction temperature, which could be due to clearing of acid and ketone groups present in the feed. Moreover, the C=O peak had at least one shoulder, which at higher wavenumbers is attributed to cyclic esters [30], for example the dimers **214b**, **198**, and **200** containing the lactone ring (Scheme 1).

Figure 8e,f also contain the fingerprint region (1500 to 500 cm^{-1}). Two weak peaks related to aromatic C=C stretch were formed at around 1600 cm^{-1} and 1480 cm^{-1} [31]. However, the interpretation was not clear, as no sp^2 C–H stretch was visible (3100–3000 cm^{-1}) nor the overtones of sp^2 C–H bend (2000–1660 cm^{-1}) [31]. However, these peaks could be overlapping sp^3 C–H and C=O stretching. The identification of aromatic compounds could be supported by the GPC UV analysis (Figure 7), which showed the formation of non-oxygen containing chromophore with a high absorption of UV wavelength 270 nm.

From the fingerprint region of the catalytic products, three major peaks decreased during the catalytic experiments: 1400 cm^{-1}, 1150 cm^{-1}, and 930 cm^{-1}. The first two could be related to acyl C–O bonds from esters and acids; the latter might be alkene sp^2 C–H bend attributed to the dimers in the feed containing C=C bonds [31]. The C=C bonds were cleared as the dimer **214a** reacted further to other dimers with catalyst. In the thermal experiments, dimer **198** with a C=C bond was produced (Figure 5); thus, the peak at 930 cm^{-1} decreased less. Less deoxygenation occurred in the thermal experiment, leading to an IR spectrum that was more similar to the dimer feed.

2.6. Product Composition by Nuclear Magnetic Resonance Spectroscopy

^{1}H nuclear magnetic resonance (NMR) spectra were recorded to study the composition of the products compared to the feed (full spectra for the LA dimer feed and a selected HDO product are presented in the Supplementary Materials, Figure S8). The NMR spectra (0.5 to 5 ppm) for the dimer feed and the products are presented in Figure 9. The two peaks that remained the same in all the experiments (3.58 and 1.73 ppm) were attributed to solvent residual signals (deuterated tetrahydrofuran, d_8–THF) [33]. The most remarkable change in the ^{1}H NMR spectra was the disappearing of two peaks at 0.87 and 0.89 ppm in the catalytic experiments, which could be related to alkyl protons [34] present in the dimer feed. New peaks emerged at 0.98 and 0.99 ppm and more peaks after 1 ppm, resulting from the diversity of alkyl protons in the products. Based on the IR results, the peak related to sp^3 C–H stretching increased with the catalyst compared to the feed,

indicating a higher total amount of methyl groups. In the thermal experiments, fewer changes were noticed in the alkyl proton peaks compared to the catalytic experiments.

Another major change can be noticed from 2 to 3 ppm. α-Protons to a carbonyl group can be seen at 2.0 to 2.7 ppm and a proton from a benzylic group can be seen at 2.2–3.0 [34]. The decreasing of peaks from 2.0 to 2.5 in the catalytic experiments most likely resulted from the removing of C=O bonds also visible in the IR spectra (Figure 8e,f).

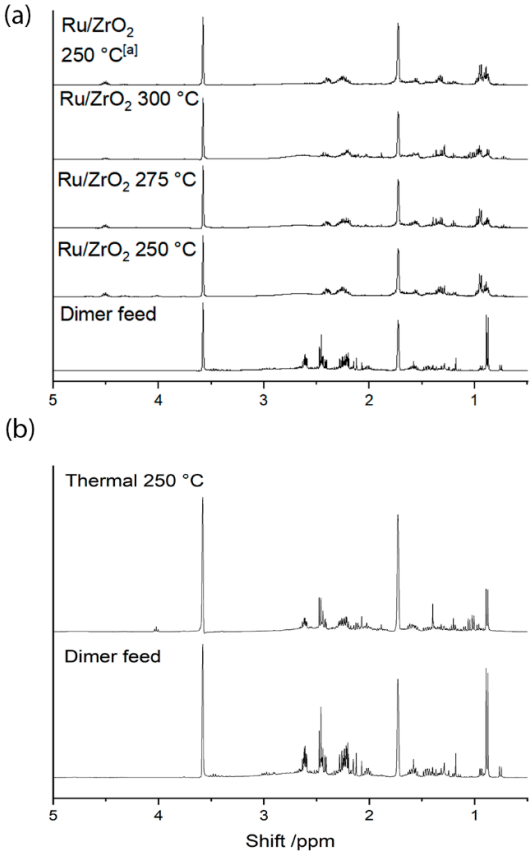

Figure 9. ^{1}H nuclear magnetic resonance (NMR) spectra (0.5–5.0 ppm) of the feed and the products obtained with (**a**) Ru/ZrO_2 catalyst and (**b**) thermally at various reaction temperatures. [a] τ_b = 1.1 g_{cat} g_{feed}^{-1} h.

Aromatic protons (Ar-H) have chemical shifts between 6.0 and 8.5 ppm [34], and the ^{1}H NMR spectra from this region for selected products and the dimer feed are presented in the Supplementary Materials, Figure S7. No aromatic hydrogen was visible in the product obtained with Ru at 250 °C, which was supported by the GPC analysis that presented no UV absorption for the sample. At higher temperatures with Ru, peaks emerged in this region.

2.7. Light and Volatile Products

Semi-quantitative yields of the main volatile product groups are presented in the Supplementary Materials (Table S2). The volatile products are understood to be those with a boiling point below 250 °C. The results were obtained from gas chromatography analysis combined with a mass spectrometer (GC-MS), and examples of the TIC chromatograms are presented in the Supplementary Materials (Figure S6). The most abundant product groups were oxygenates, such as ketones, acids, and esters, rather than hydrocarbons (HC). The highest yields of aliphatic hydrocarbons (including linear, branched, and cyclic HCs) were produced with Ru at 300 °C, and it seems that an increasing trend in aliphatic hydrocarbon yields existed with increasing reaction temperature. Moreover, the higher the

reaction temperature, the more olefins were formed (based on GC-MS identification), although the total amount for HCs remained low (Tables S1 and S2). The observation of olefins could partly explain the decrease of the H/C ratio in Figure 6; however, the detection of sp^2 C–H bend (900–1000 cm^{-1}) with IR was difficult due to the complexity of the obtained products, and no confirmation for the olefins was obtained from other analysis methods. Since most of the volatile products were oxygenates at ≤300 °C, an experiment with higher batch residence time (1.1 g_{cat} h g_{feed}^{-1}) was performed with the Ru catalyst at 250 °C. However, no significant difference was achieved in the hydrocarbon yields (Table S2). The high share of oxygenates highlights the importance of catalyst development if a one-pot process from LA dimers to hydrocarbons is preferred. Alternatively, a two-step HDO process proposed by Myllyoja et al. [35] could be developed.

Another important observation that can be made from the GC-MS analysis is the formation of aromatic compounds at higher temperatures. At 250 °C, no aromatics were observed with the Ru catalyst, which was also supported by the GPC UV analysis, as Figure 7c presents no UV absorbance typical for aromatics at 270 nm. No aromatics were detected with ^{1}H NMR either (Figure S7). The formation of UV chromophores increased with temperature (Figure 7c), which could mean a higher amount of aromatic products. With Ru, aromatics were detected at temperatures higher than 250 °C (Table S2). The formation of aromatics with the catalyst at high temperature could have been caused by the dehydrogenation of the various cyclic compounds that were formed from the LA dimers (Table S1). In the literature, high temperatures have been found to promote cyclohexane dehydrogenation on Ru catalysts [36,37]. Thermally, especially ketones were formed. However, the compounds causing the UV absorbance in Figure 7d remained unclear, as the thermal experiment provided relatively high peaks even without detected aromatics by GC-MS or ^{1}H NMR, which could indicate the formation of another UV chromophore that is non-aromatic (perhaps a conjugated system).

Some of the main volatile products detected in the product mixtures are presented in Scheme 2. The compounds produced in Reactions 2–4.1 were the most abundant products in the groups of esters, acids, and hydrocarbons. Another significant product was γ-valerolactone (GVL) from Reaction 1, but it formed over Ru from the unreacted levulinic acid still present in the feed. As the pentanoic acid from Reaction 3.1 was not detected from the product mixtures, the formation of GVL from dimer **200** was not likely. Reactions 2 and 3.2 present two product components. The ones in brackets (OSD and GNL) were identified in the product mixtures using the MS spectral database. However, as the match factors were poor (Table S1), similar compounds (not included in MS database) were proposed based on the decarboxylation from dimers **198** or **200**. The differences between the proposed compounds and the identified ones are very slight, so the compounds could have been easily misidentified based on retention time and MS match. Among the aromatic compounds, 5-hydroxy-2,3,4-trimethylacetophenone was the most abundant volatile compound. As a conclusion, most of the detected volatile compounds were cyclic oxygenates. The GC-MS TIC chromatograms of selected HDO products are presented in the Supplementary Materials (Figure S6 and Table S1).

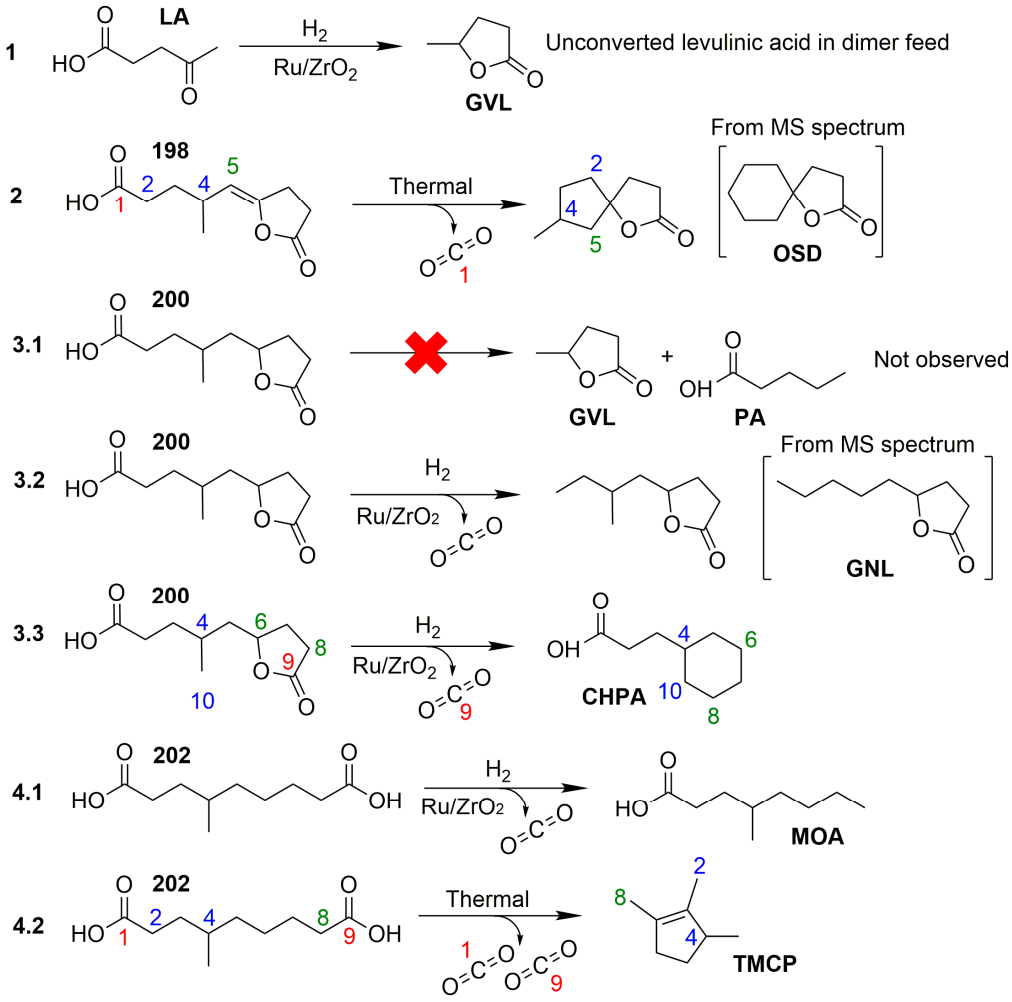

Scheme 2. Suggested formation of selected volatile products. LA: levulinic acid, GVL: γ-valerolactone, OSD: 1-oxaspiro(4,5)decan-2-one, PA: pentanoic acid, GNL: γ-nonalactone, CHPA: cyclohexanepropanoic acid, MOA: 4-methyloctanoic acid, TMCP: 1,2,3-trimethylcyclopentene.

Water yields are presented in Table S2. In the Ru experiments, the highest amount of water was produced at 250 °C, and the water yield decreased at higher temperatures, indicating relatively less HDO. The increase of batch residence time also increased the water yield by ca. 2 percentage points.

Gas phases were analyzed after the Ru experiments and the thermal experiment, and they consisted mainly three components: unreacted hydrogen, CO_2, and methane (Supplementary Materials, Table S3). In the thermal experiment, almost no methane was detected. In the catalytic experiments, the amount of methane decreased by increasing reaction temperature, which was surprising. It is most likely due to how the batch reactor was operated, as hydrogen was replenished whenever the reactor pressure had decreased five bars from the initial pressure. At high reaction temperature (≥300 °C), decarboxylation was so significant that the reactor pressure did not drop and no hydrogen could be replenished, which could explain the lower level of methane detected in the gas phase after the experiment and the increased production of olefins with Ru at 300 °C. A small amount of CO was also detected in the gas phases; thus, the water gas shift (WGS) reaction could have occurred. The WGS equilibrium constants and equilibrium compositions were calculated via HSC Chemistry 9.7 software. The calculations showed that the formation of CO_2 through WGS was not favorable in the used conditions (50 bar H_2, 250 to 350 °C). Thus, most of the CO_2 likely formed through decarboxylation, which could explain the formation of many of the major volatile products (Scheme 2). With Ru catalysts, it can be stated that HDO was preferred at a low reaction temperature producing water, but at higher temperatures, decarboxylation became more favorable as more CO_2

was formed. Methane and other light hydrocarbons were also detected from the Ru product gases, which could form through methanation, C–C coupling, or cracking.

A comparison of the thermal experiment to the catalyzed experiments can clarify which reactions occurred thermally and for which reactions the catalyst was responsible. Firstly, the decarboxylation of LA dimers occurred thermally, although it was enhanced by the catalyst (Section 2.5). Thus, the ketones that were produced thermally (Table S2) could have been formed by the decarboxylation of e.g., dimers 214a and 216 on both ends, leaving behind a C_8 ketone. Furthermore, the high formation of dimer 198 from dimer 216 in the thermal experiment indicates that an intramolecular cyclization could occur thermally, which would explain the thermal formation of 1,2,3-trimethylcyclopentene (TMCP) and 1-oxaspiro(4,5)decan-2-one (OSD) (Scheme 2). TMCP and OSD were formed to a much lesser extent in the catalytic experiment at 250 °C than in the thermal experiment at 250 °C (Figure S6 no. 1 and 14). Thus, TMCP and OSD might have been formed only thermally, simultaneously to the catalyzed reactions. All the other reactions illustrated in Scheme 2 occurred only on the catalyst. The catalyst was responsible for the formation of acids (especially cyclohexanepropanoic acid (CHPA)) and esters (especially lactones).

In a similar HDO study with Angelica lactone dimer, Mascal et al. [5] were able to reach 88% molar yield of total hydrocarbons, of which C_{10} was the main alkane with Ir–ReO_x/SiO_2 catalyst. Moreover, the authors did not report the identification of any cyclic products but only branched linear HCs. Li et al. [12] were able to obtain 94% hydrocarbon yield (including linear and branched paraffins and cycloparaffines) via HDO of the HAA product of 2-methylfuran using an acidic Pt/ZrP catalyst. Similarly, Corma et al. [13] reached 87% diesel yield (including C_9-C_{24} linear, branched, cyclic, and aromatic HCs) after hydrogenating the HAA product of 2-methylfuran with Pt/C catalyst. The Dumesic research group has produced HCs up to C_{15} from aldol crossed-condensation products of furfural or HMF with acetone with a Pt/SiO_2-Al_2O_3 catalyst [8]. They have also produced C_8-C_{16} alkenes with a yield over 70% via butene oligomerization (no hydrotreatment step) with a zeolite or Amberlyst 70 catalyst [16]. Overall, the noble metal catalysts have proven their capability in the HDO of extended carbon chains (>C_6) produced from biomass. These results from the literature are closer to full deoxygenation than ours with Ru, as we obtained mainly oxygenated products. We also obtained cyclic products as some of the other authors [12,13]. All of the tested molecules in literature contained lactone or furan structures, but the LA dimers we tested contained acid, ketone, and lactone structures sometimes in the same molecule, thus being more complex in structure. Mascal et al. [5] explained that the addition of Re to a noble metal catalyst should increase the activity to CO hydrogenolysis. Moreover, their catalyst (Ir–ReO_x) was found to be active in lactone HDO as well. In our earlier studies, we found Ru to be the most active noble metal toward hydrocarbons from GNL [24]. However, the catalyst was not as active with the LA dimer feed; thus, an interesting option would be to add a reducible promotor (e.g., Re or Ti) to the catalyst.

3. Materials and Methods

3.1. Materials

The LA dimer mixture was prepared as described by Käldström et al. [7], who used a 0.7% Pd catalyst on Amberlyst CH28 ion-exchange resin at 120 °C to convert LA into dimers via aldol self-condensation in a fixed-bed reactor under hydrogen pressure. The chemicals in the analytics were obtained from Sigma-Aldrich and used without further purification: nonanoic acid (98%), tetrahydrofuran (LiChrosolv®, ≥99.9%), tetrahydrofuran-d_8 (99.5 atom.% D), 2-butanol (99%), 2-propanol (≥99.5%), acetonitrile (Riedel-de Haën, 99.90%), formic acid (VWR Chemicals, 99%), levulinic acid (Merck, for synthesis), azelaic acid (Alfa Aesar, 96%), dodecanedioic acid (Fluka, ≥98%), and stearic acid (>99%). Monoclinic ZrO_2 catalyst support was obtained from Saint-Gobain NorPro, and the metal precursor was Ru(III) nitrosylnitrate (Alfa Aesar, ≥31.3 wt.% Ru). The Karl–Fisher titration chemicals were Merck's Apura® two component titrant containing MeOH and iodine, Merck's Apura® solvent for volumetric Karl–Fisher titration containing MeOH and imidazole, and Merck's Apura® water standard (1% H_2O).

All gases used in the experiments were purchased from Oy AGA (Aktiebolaget Gasaccumulator) Ab. H_2 (purity 5.0) was used in the HDO experiments, and the gases used in analytics were H_2 (purity 5.0), He (purity 4.6), Ar (purity 5.0), synthetic air (purity 5.0), N_2 (purity 5.0), O_2 (purity 5.0), and a mixture of 2% H_2 (purity 5.0) in Ar (purity 5.0). Two calibration gas mixtures were utilized from Oy AGA Ab. The first one contained 40 mol.% N_2, 5 mol.% CH_4, 10 mol.% C_2H_6, 5 mol.% C_2H_4, 10 mol.% C_3H_8, 5 mol.% C_3H_6, 5 mol.% C_2H_2, 10 mol.% C_4H_{10}, and 10 mol.% isobutane. The second calibration gas mixture contained 15 vol.% CO, 15 vol.% CO_2, 15 vol.% H_2, 40 vol.% N_2, and 15 vol.% CH_4. Detailed information on the providers of all the reagents and gases are listed in Table S5 in the Supplementary Materials.

3.2. Catalyst Preparation

The monoclinic ZrO_2 support was ground and sieved to 0.15–0.3 mm prior to calcination in synthetic air at 600 °C for 10 h (heating rate 100 °C h^{-1}). Prior to metal impregnation, the water uptake capacity of the support was determined via titration with deionized water. The typical catalyst preparation procedure was as follows: Ru was added to the support (4 g) by incipient wetness impregnation using an appropriate amount of aqueous solution of the metal precursor (0.422 g of Ru nitrosylnitrate dissolved to 1.212 g of deionized water). A few extra drops of water were used to flush all the precursor solution from the used beaker to the catalyst. During the room temperature impregnation, stirring was conducted manually by shaking the catalyst beaker after every few drops of precursor solution added during the 20 to 30 min time period. At the end of the impregnation, a spatula was used to gently mix the wet catalyst. After impregnation, the catalyst was dried at room temperature for 5 h and in a 100 °C oven overnight. Thermal treatment for the catalyst was performed at 350 °C for 3 h with a heating ramp of 30 °C h^{-1} under a flow of synthetic air (100 mL min^{-1}). The term 'fresh, thermally treated catalyst' refers to the catalyst obtained after this process, i.e., before reduction. The nominal amount of Ru on the support was 3.2 wt %.

3.3. Catalyst Characterization

XRF was used to determine the Ru content of the prepared catalyst. The equipment was a Rigaku ZSX Primus wavelength dispersive spectrometer. A tablet was prepared into an aluminum cup by grinding the samples and pressing it with Boreox® binder.

Nitrogen physisorption measurement at −196 °C in liquid nitrogen was conducted with a Thermo Scientific Surfer equipment. The catalyst sample (300 mg) was weighted into a quartz tube and evacuated at 300 °C for 3 h prior to the measurement. The Brunauer–Emmett–Teller (BET) [38] specific surface area was calculated from the adsorption isotherm, and the pore volume and average pore diameter were calculated from the desorption isotherm according to the BJH method [39].

Hydrogen chemisorption at 75 °C was performed for the Ru/ZrO_2 catalyst as suggested by Shen et al. [40] using Thermo Scientific Surfer equipment. Prior to the analysis, the catalyst sample (300 mg) was reduced in hydrogen flow at 290 °C for 3 h (heating rate 5 °C min^{-1}) and degassed in the same temperature for 2 h. The total adsorption isotherm was measured first, after which the sample was evacuated down to 10^{-5} Torr, and the reversible adsorption isotherm was measured. The irreversible monolayer volume was obtained from the linear regression of the subtracted isotherm to zero pressure. The dispersion and metal particle size were calculated from the irreversible monolayer volume assuming spherical particles and gas–metal stoichiometry of 2:1 as described by [41].

Scanning transmission electron microscopy images were taken from the fresh, thermally treated catalyst on a JEOL JEM-2200FS double aberration corrected, high-resolution microscope, operated at 200 kV acceleration voltage. The microscope is equipped with an X-ray EDS detector for chemical elemental analysis in the sample. The samples were drop-casted using ethanol onto a copper grid coated with ultrathin (<10 nm) holey carbon thin film.

Temperature-programmed reduction experiments were performed using an Altamira AMI-200 connected to a TCD and to an OmniStar™ mass spectrometer by Pfeiffer Vacuum. The catalyst (50 mg) was placed in a U-shaped quartz reactor, pre-dried in He (40 mL min^{-1}) at 350 °C for 1 h, and cooled to 30 °C. For the TPR, the catalyst was heated at 10 °C min^{-1} in 2% H_2/Ar (46.3 mL min^{-1}) up

to 350 °C, held for 2 h at 350 °C, and cooled to 30 °C. The catalyst was kept overnight at room temperature in 5 mL min^{-1} He. Afterwards, the catalyst was opened to the atmosphere for 20 min and sealed again. The pre-drying and TPR steps were repeated as before, except that the hold at 350 °C in 2% H_2/Ar was only 10 min. For comparison, the whole procedure was repeated with a fresh sample of catalyst, except that the opening to the atmosphere was omitted.

Thermogravimetric analysis was performed with a TA Instruments' TGA Q500 equipment. Since the spent catalysts were soaked in the liquid dimer HDO products, an evaporation step in N_2 had to precede the combustion step. In order to determine the fraction of liquid lost during evaporation, the dimer feed and the HDO products were tested in TGA with the same procedure as the catalysts. First, the sample was heated to 300 °C in N_2 at 10 °C min^{-1} and held for 5 min. Afterwards, the sample was cooled to 30 °C in N_2 and held for 5 min. Finally, the gas was switched to O_2, and the temperature was ramped up at 10 °C min^{-1} to 900 °C and held for 5 min. Detailed information on the providers of characterization instruments and equipment are listed in Table S6 in the Supplementary Materials.

3.4. HDO Experiments

Batch experiments were conducted in a 50 mL Parr reactor with a borosilicate liner. The experiments were conducted as slurry in liquid phase without solvent, and the reaction time was about 5 h. Prior to the experiments, 1.0 or 2.0 g of Ru/ZrO_2 catalyst was dried at 120 °C for 1 h and reduced at 350 °C with 60 bar H_2 and 100 rpm mixing for 2 h in situ. After reduction, the reactor was cooled to room temperature, H_2 pressure was released, and the reactor was flushed with N_2. The reactor was opened, and an appropriate amount of feed (see Supplementary Materials, Table S3) melted at 70 °C was added to the liner, after which the reactor was closed again and flushed with H_2. The reactor was heated to 250 °C temperature, after which stirring of 400 rpm was started and 50 bar H_2 was added. Hydrogen was always added at 250 °C, regardless of the final reaction temperature to avoid thermal reactions during the heating. H_2 was replenished during the reaction each time the pressure had decreased by 5 bar. Finally, the reactor was cooled down, after which the gas phase was sampled for analysis from the reactor's lines into an evacuated sampling bomb. Then, the reactor was vented and opened in order to collect the other products. Mass loss for the experiments was between 1% and 5%, except for the experiment made at 300 °C, for which the mass loss was 10% (Supplementary Materials, Table S3). According to Reynolds number calculations (Supplementary Materials, Table S4), the stirring created a flow inside the vessel at the lower limit of turbulence. Assuming that turbulence provides adequate mixing, the mixing in the vessel was likely sufficient.

The amount of feed in the batch reactor was chosen to allow the greatest possible head space for H_2, yet ensuring that the impeller would be fully submerged in the liquid. The necessary amounts were calculated from the density of the feed at 50 °C, 1162 kg m^{-3}, and adjusted for an estimated thermal expansion. The thermal expansion was estimated with the TRIDEN equation using the coefficients obtained for levulinic acid by Guerrero et al. [42] According to these criteria, 9.4 g were fed for the 250 °C experiment, 9.2 g were fed for the 275 °C experiment, and 9.0 g were fed for the 300 °C experiment.

3.5. Product Analytics

High-performance liquid chromatography was used to estimate the consumption of the individual dimers (Scheme 1). Each sample and the feed were diluted to 50/50 wt % MilliQ water/acetonitrile (ACN) solution, which contained 100 ppm nonanoic acid as a standard. The final concentration of each sample was approximately 100 ppm. The equipment was an Agilent 1260 HPLC-system coupled to an Agilent 6530 QTOF mass spectrometer with electrospray source (ESI). For chromatographic separation, a Luna Omega PS-C18 column (100 × 2.1 mm, 3 μm) was used with solvents: (A) MilliQ water with 0.1% formic acid and (B) ACN with 0.1% formic acid. A flow rate of 0.4 mL min^{-1} and an injection volume of 5 μL were used. The applied gradient was 0–5 min 5% B to 95% B followed by 5–10 min back to 5% B. Mass chromatograms were recorded as TIC in mass range of 50–1100 m/z with negative mode (–ESI). For searching the individual dimers, extracted ion

chromatograms (EIC) were recorded for selected molecular masses (**214**, **216**, **202**, **200** and **198** amu). The following settings were used: capillary 3000 V; nebulizer 40 psig; N_2 drying gas 13 L min^{-1}; gas temperature 300 °C; fragmentor 140 V; skimmer 65 V and octopol 600 V.

Light/volatile organic products were identified using an Agilent GC equipped with a Zebron ZB-wax Plus column (60 m × 250 μm × 0.25 μm) and a mass spectrometer (GC-MS, 7890-5975). A 20 wt % dilution of each sample was made in 2-butanol. Approximately 2 wt % of 2-propanol was added as an internal standard. Then, 1 μL of each solution was injected at 250 °C with 0.6 mL min^{-1} flow and an 80:1 split ratio. The temperature program started with a 2 min hold at 60 °C, followed by heating to 160 °C (7 °C min^{-1}) with a 3 min hold, heating to 200 °C (5 °C min^{-1}) with a 6 min hold, and finally heating to 250 °C (10 °C min^{-1}) with a 15 min hold. The electron impact ionization MS detector was operated at 70 eV with a quadrupole scan range of 30–500 amu. The NIST (U.S. National Institute of Standards and Technology) mass spectral library was used to aid spectral interpretation.

Gel permeation chromatography was used to estimate molecular sizes. The equipment was an Agilent 1100 HPLC system consisting of UV and RI detectors and a Phenogel 50 Å column (5 μm × 300 × 7.8 mm). Each sample (0.1 g) was dissolved to 1 g of tetrahydrofuran, which was also used as an eluent with a flow rate of 1 mL min^{-1}. The column temperature was 35 °C, and the injection volume was 20 μL. The RI detector temperature was 30 °C, and the UV detection was measured at 270 nm.

^1H nuclear magnetic resonance spectra were recorded with a Bruker AVANCE-III 400 MHz spectrometer operating at 400.13 MHz for ^1H. Samples were dissolved in deuterated tetrahydrofuran (approximately 1 mg of sample per 1 mL of d_8-THF) in 5 mm NMR tubes at 22 °C. For all the ^1H NMR spectra, the reference value of one of the solvent residual signals (3.58) [33] was used to correct the peak positions.

Infrared spectroscopy was used for qualitative analysis of the feed and the liquid products. The equipment was a Perkin Elmer Spectrum Two equipped with an attenuated total reflection (ATR) crystal having a refractive index of 2.4 at a wave number of 1000 cm^{-1}. The penetration depth was 2.0 um for samples with a refractive index of 1.5 at a wave number of 1000 cm^{-1}. Prior to the analysis, the background was measured.

Van Krevelen diagrams [28] were constructed based on the elemental compositions of the organic phases and analyzed with a Perkin Elemer 2400 Series II elemental analyzer. The results were corrected for the presence of dissolved or colloidal water.

A separate aqueous phase (if any) was separated using a separating funnel and analyzed with GC-MS as described earlier (injection volume 0.5 μL and a quadrupole scan range of 18–500 amu). The pH of the aqueous phases were measured using a pH paper. The dissolved or colloidal water in the organic phase was determined by an SI Analytics' volumetric Karl-Fisher titrator (TitroLine 7500 KF). A water standard was used to calibrate the concentration of the titrant before the measurement. The total water was calculated as a sum of aqueous phase and water trapped in the organic phase, and it was assumed to be 100% H_2O, although traces of acetic, propionic, and butyric acids, 3-methylcyclopentanone, butyrolactone, GNL, and GVL were detected by the GC-MS.

The product gas from the batch reactor was analyzed by an Agilent 6890 Series GC with a flame ionization detector (FID) and a TCD. The TCD was connected to two columns: an HP-PLOT/Q (30 m × 0.53 mm × 40 μm) and an HP Molesieve (30 m × 0.53 mm × 25 μm), and it was used to analyze CO, CO_2, H_2, and N_2. Hydrocarbons were analyzed with the FID utilizing a HP-AL/KCL column (50 m × 0.32 m × 8 μm). Prior to the measurements, the GC was calibrated with an Oy AGA Ab calibration gas mixture. The inlet temperature was 200 °C, and the columns were heated from 40 to 200 °C (10 °C min^{-1}). Detailed information on the providers of the analytical instruments and equipment are listed in Table S6 in the Supplementary Materials.

4. Calculations

The LA dimers relative change was estimated from the HPLC analysis of the feed mixture and the products. Each sample was analyzed three times, and the final estimation was an average of the three measurements. The mass fraction of each component was calculated using Equation (1), after which the semi-quantitative estimation of relative change was conducted with Equation (2).

$$P_i = \frac{F_i A_i P_s}{A_s} \quad (1)$$

$$X = \frac{P_i - P_{i0}}{P_{i0}} \quad (2)$$

In Equations (1) and (2), F_i is the response factor for component *i*, A_i is the peak area of component *i*, P_s is the mass fraction of standard, A_s is the peak area of standard, and P_{i0} is the mass fraction of component *i* in the feed. The peak area for each dimer (A_i) was obtained from the extract ion chromatograms of the masses related to each dimer. The response factors were assumed to be one due to a lack of calibration (standards unavailable).

The mass fractions of volatile components were estimated from the GC-MS analysis according to Equation (1). The F factors for selected components were obtained based on calibrations or calculated as described by Scanlon [43]. An average F factor was calculated and used for all the products without further calibration, since most of the standards were unavailable. Thus, the semi-quantitative yields were obtained from Equation (3).

$$Y = \frac{m_i}{m_f} \quad (3)$$

Here, m_i is the mass of component *i* in the product mixture, and m_f is the mass of total organic feed put in the reactor.

The concept of batch residence time (τ_b, Equation (4)) [44,45] was applied instead of reaction time, as different amounts of dimer feed were weighed in each experiment due to expected thermal expansion, such that enough volume would be available for the gas. Furthermore, reporting relative values instead of reaction time has been recommended for catalytic experiments, as results vary in different reaction setups [46,47].

$$\tau_{\mathrm{b}} = \frac{m_{\mathrm{cat}} t}{m_{\mathrm{f}}} \quad (4)$$

Here, m_{cat} is the mass of catalyst added to the reactor and *t* is the reaction time.

The mass losses determined in the TGA tests were used to calculate the amounts of solid deposits on the spent catalysts. The fraction of liquid lost in the evaporation step with N_2 was assumed to be the same in both of the tests with pure dimer products and in the tests with soaked, spent catalysts. The evaporated product fraction ($f_{v,DIM}$) was determined with the TGA of the dimer products as:

$$f_{v,DIM} = \frac{m_{DIM,0} - m_{DIM,i}}{m_{DIM,0}}, \quad (5)$$

where $m_{DIM,0}$ is the mass of dimer product loaded to the TGA pan, and $m_{DIM,i}$ is the mass left after the evaporation step. The mass of liquid dimer products ($m_{DIM/C}$) present in the soaked, spent catalysts loaded to the TGA pan ($m_{cat,0}$) was determined as:

$$m_{DIM/C} = \frac{m_{cat,0} - m_{cat,i}}{f_{v,DIM}}, \quad (6)$$

where $m_{cat,i}$ is the mass left after the evaporation step with the TGA of the soaked catalysts. The mass of the final dry catalyst ($m_{cat,f}$) was the mass left after combustion. The mass of solid deposits (m_s) was assumed to be:

$$m_s = m_{cat,0} - m_{DIM/C} - m_{cat,f}. \quad (7)$$

The solid deposits are reported as the ratio $m_s/m_{cat,f}$.

5. Conclusions

In this study, the potential of LA dimers as a source of bio-based products via HDO was demonstrated for the first time using a zirconia-supported ruthenium catalyst. The hydrodeoxygenation of LA dimers was performed in a batch reactor at 250 to 300 °C and 50 bar H_2. In the catalytic experiments, the double bonds in the more unsaturated dimers (**214a**, **214b**, and **216**)

were hydrogenated, and the ketone moieties were removed (dimer **202**) or intramolecularly lactonized (dimer **200**). On the other hand, the thermal experiment favored lactonization without further hydrogenation (dimer **198**).

Deoxygenation increased with increasing reaction temperature, which was evidenced by the elemental analysis and the decrease of the C=O peak in infrared spectra. Oxygen was removed as water and CO_2. Other minor changes were the oligomerization via condensation and the formation of aromatic compounds at high temperatures. Thus, temperature optimization is required to enhance oxygen removal while avoiding oligomerization.

The volatile products consisted mainly of acids, esters, and ketones, but also linear, branched, and cyclic hydrocarbons. At a higher batch residence time (τ_b = 1.1 g_{cat} g_{feed}^{-1} h), the formation of hydrocarbons did not increase significantly. By contrast, at higher temperatures, more volatiles were formed. The volatiles were formed mainly after the decarboxylation of dimer molecules. This study demonstrates for the first time the potential of LA dimers as a route from lignocellulosic biomass to sustainable biofuels and biocomponents.

Supplementary Materials: The following are available online at www.mdpi.com/xxx/s1, Figure S1: Bright-field STEM image and corresponding EDS, Figure S2: Dark-field STEM images, Figure S3: EDS corresponding to Figure S2, Figure S4: TPR graphs, Figure S5: TIC chromatograms, Figure S6: TIC chromatograms, Table S1: Compounds identified from GC-MS TIC chromatograms, Table S2: Semi-quantitative volatile liquid product yields, Figure S7: ^{1}H NMR spectra (6.0–8.0 ppm), Figure S8: Full-scale ^{1}H NMR spectra, Table S3: Mass balances and gas phase compositions, Table S4: Physical properties, Table S5: Providers of reagents and gases, and Table S6: Providers of instruments and equipment.

Author Contributions: Conceptualization, E.M., J.L.G.E., M.L., M.K., and R.K.; Investigation: E.M., J.L.G.E., H.M.-T., and H.J.; Methodology: E.M., J.L.G.E., H.M.-T., and H.J.; Visualization: E.M. and J.L.G.E.; Writing—original draft: E.M. and J.L.G.E.; Writing—reviewing and editing: E.M., J.L.G.E., M.L., M.K., H.M.-T., H.J., R.L.P., and R.K.; Supervision: R.L.P. and R.K.

Funding: This research was funded by Neste Corporation. E.M. further acknowledges a grant from Aalto University; J.L.G.E. grants from Fortum Foundation (no. 201800142) and from the Finnish Foundation for Technology Promotion (no. 6712).

Acknowledgments: The authors are grateful to Steven Spoljaric, Sami Lipponen, and Jari Koivisto for the NMR analysis, Tiia Viinikainen for helping with ATR IR, Aitor Arandia Gutiérrez for helping with TPR, Elias Ikonen for sharing GC-MS method for LA dimers, Johanna Helminen for conducting the XRF measurement, and Aalto University's BioEconomy and Raw materials research infrastructures and OtaNano nanomicroscopy center are acknowledged for equipment support.

Conflicts of Interest: The authors declare no conflict of interest.

References

1. Oh, Y.K.; Hwang, K.R.; Kim, C.; Kim, J.R.; Lee, J.S. Recent developments and key barriers to advanced biofuels: A short review. *Bioresour. Technol.* **2018**, *257*, 320–333.
2. Naik, S.N.; Goud, V.V.; Rout, P.K.; Dalai, A.K. Production of first and second generation biofuels: A comprehensive review. *Renew. Sustain. Energy Rev.* **2010**, *14*, 578–597.
3. Werpy, T.; Petersen, G. *Top Value Added Chemicals from Biomass Volume I—Results of Screening for Potential Candidates from Sugars and Synthesis Gas*; National Renewable Energy Lab.: Golden, CO, USA, 2004; p. 76.
4. Isikgor, F.H.; Becer, C.R. Lignocellulosic biomass: A sustainable platform for the production of bio-based chemicals and polymers. *Polym. Chem.* **2015**, *6*, 4497–4559.
5. Mascal, M.; Dutta, S.; Gandarias, I. Hydrodeoxygenation of the angelica lactone dimer, a cellulose-based feedstock: Simple, high-yield synthesis of branched C7-C10 gasoline-like hydrocarbons. *Angew. Chem. Int. Ed.* **2014**, *53*, 1854–1857.
6. Bond, J.Q.; Upadhye, A.A.; Olcay, H.; Tompsett, G.A.; Jae, J.; Xing, R.; Alonso, D.M.; Wang, D.; Zhang, T.; Kumar, R.; et al. Production of renewable jet fuel range alkanes and commodity chemicals from integrated catalytic processing of biomass. *Energy Environ. Sci.* **2014**, *7*, 1500–1523.
7. Käldström, M.; Lindblad, M.; Lamminpää, K.; Wallenius, S.; Toppinen, S. Carbon Chain Length Increase Reactions of Platform Molecules Derived from C5 and C6 Sugars. *Ind. Eng. Chem. Res.* **2017**, *56*, 13356–13366.

8. Huber, G.W.; Chheda, J.N.; Barrett, C.J.; Dumesic, J.A. Production of Liquid Alkanes by Aqueous-Phase Processing of Biomass-Derived Carbohydrates. *Science* **2005**, *308*, 1446–1450.
9. West, R.M.; Liu, Z.Y.; Peter, M.; Dumesic, J.A. Liquid alkanes with targeted molecular weights from biomass-derived carbohydrates. *ChemSusChem* **2008**, *1*, 417–424.
10. Wilson, J.; Chen, E.Y.X. Organocatalytic Cross-Coupling of Biofuranics to Multifunctional Difuranic C11 Building Blocks. *ACS Sustain. Chem. Eng.* **2016**, *4*, 4927–4936.
11. Zang, H.; Chen, E.Y.X. Organocatalytic upgrading of furfural and 5-hydroxymethyl furfural to C10 and C12 furoins with quantitative yield and atom-efficiency. *Int. J. Mol. Sci.* **2015**, *16*, 7143–7158.
12. Li, G.; Li, N.; Wang, Z.; Li, C.; Wang, A.; Wang, X.; Cong, Y.; Zhang, T. Synthesis of high-quality diesel with furfural and 2-methylfuran from hemicellulose. *ChemSusChem* **2012**, *5*, 1958–1966.
13. Corma, A.; De La Torre, O.; Renz, M. Production of high quality diesel from cellulose and hemicellulose by the Sylvan process: Catalysts and process variables. *Energy Environ. Sci.* **2012**, *5*, 6328–6344.
14. Serrano-Ruiz, J.C.; Wang, D.; Dumesic, J.A. Catalytic upgrading of levulinic acid to 5-nonanone. *Green Chem.* **2010**, *12*, 574.
15. Serrano-Ruiz, J.C.; Braden, D.J.; West, R.M.; Dumesic, J.A. Conversion of cellulose to hydrocarbon fuels by progressive removal of oxygen. *Appl. Catal. B Environ.* **2010**, *100*, 184–189.
16. Bond, J.Q.; Alonso, D.M.; Wang, D.; West, R.M.; Dumesic, J. a Integrated Catalytic Conversion of γ-Valerolactone to Liquid Alkenes for Transportation Fuels. *Science* **2010**, 1110–1114.
17. Grilc, M.; Likozar, B. Levulinic acid hydrodeoxygenation, decarboxylation and oligmerization over NiMo/Al2O3 catalyst to bio-based value-added chemicals: Modelling of mass transfer, thermodynamics and micro-kinetics. *Chem. Eng. J.* **2017**, *330*, 383–397.
18. Blessing, R.W.; Petrus, L. A Catalytic Process for the Dimerization of Levulinic Acid and the Preparation of Diesters from these Dimers Obtainable by such Process. WO 2006/056591 A1, 1.6.2006; p. 29.
19. Faba, L.; Díaz, E.; Ordóñez, S. Base-Catalyzed Condensation of Levulinic Acid: A New Biorefinery Upgrading Approach. *ChemCatChem* **2016**, *8*, 1490–1494.
20. Li, Z.; Zhang, J.; Nielsen, M.M.; Wang, H.; Chen, C.; Xu, J.; Wang, Y.; Deng, T.; Hou, X. Efficient C-C Bond Formation between Two Levulinic Acid Molecules to Produce C 10 Compounds with the Cooperation Effect of Lewis and Brønsted Acids. *ACS Sustain. Chem. Eng.* **2018**, *6*, 5708–5711.
21. Amarasekara, A.S.; Wiredu, B.; Grady, T.L.; Obregon, R.G.; Margetić, D. Solid acid catalyzed aldol dimerization of levulinic acid for the preparation of C10 renewable fuel and chemical feedstocks. *Catal. Commun.* **2019**, *124*, 6–11.
22. Cornils, B.; Lappe, P.; by Staff, U. Dicarboxylic Acids, Aliphatic. In *Ullmann's Encyclopedia of Industrial Chemistry*; Wiley-VCH Verlag GmbH & Co. KGaA: Weinheim, Germany, 2014; pp. 1–18.
23. Van den Brink, P.J.; von Hebel, K.L.; Lange, J.-P.; Petrus, L. A Process for the Hydrogenation of a Lactone or of a Carboxylic Acid or an Ester having a Gamma-Carbonyl Group. WO2006067171, 29.6.2006; pp. 1–11.
24. González Escobedo, J.L.; Mäkelä, E.; Braunschweiler, A.; Lehtonen, J.; Lindblad, M.; Puurunen, R.L.; Karinen, R. Solvent-free Hydrodeoxygenation of γ-Nonalactoneon Noble Metal Catalysts Supported on Zirconia. *Top. Catal.* **2018**, *62*, 724–737.
25. Chia, M.; Pagán-Torres, Y.J.; Hibbitts, D.; Tan, Q.; Pham, H.N.; Datye, A.K.; Neurock, M.; Davis, R.J.; Dumesic, J.A. Selective hydrogenolysis of polyols and cyclic ethers over bifunctional surface sites on rhodium-rhenium catalysts. *J. Am. Chem. Soc.* **2011**, *133*, 12675–12689.
26. Bie, Y.; Gutierrez, A.; Viljava, T.R.; Kanervo, J.M.; Lehtonen, J. Hydrodeoxygenation of Methyl Heptanoate over Noble Metal Catalysts: Catalyst Screening and Reaction Network. *Ind. Eng. Chem. Res.* **2013**, *52*, 11544–11551.
27. Jung, K.T.; Bell, A.T. The effects of synthesis and pretreatment conditions on the bulk structure and surface properties of zirconia. *J. Mol. Catal. A Chem.* **2000**, *163*, 27–42.
28. van Krevelen, D.W. Graphical-statistical method for the study of structure and reaction processes of coal. *Fuel* **1950**, *29*, 269–283.
29. Leitner, W.; Klankermayer, J.; Pischinger, S.; Pitsch, H.; Kohse-Höinghaus, K. Advanced Biofuels and Beyond: Chemistry Solutions for Propulsion and Production. *Angew. Chem. Int. Ed.* **2017**, *56*, 5412–5452.
30. Field, L.D.; Sternhell, S.; Kalman, J.R. *Organic Structures from Spectra*, 5th ed.; Field, L.D., Sternhell, S., Kalman, J.R., Eds.; John Wiley & Sons, Ltd.: West Sussex, England, 2013; p. 497.
31. Beauchamp, P. Spectroscopy Tables. Available online: https://www.cpp.edu/~psbeauchamp/pdf/spec_ir_nmr_spectra_tables.pdf (accessed on 2 December 2019).

32. Coates, J. Interpretation of Infrared Spectra, A Practical Approach. In *Encyclopedia of Analytic Chemistry: Applications, Theory and Instrumentation*; John Wiley & Sons Ltd., Meyers, R.A., Eds.; 2006; pp. 10815–10837.
33. Fulmer, G.R.; Miller, A.J.M.; Sherden, N.H.; Gottlieb, H.E.; Nudelman, A.; Stoltz, B.M.; Bercaw, J.E.; Goldberg, K.I. NMR Chemical Shifts of Trace Impurities: Common Laboratory Solvents, Organics, and Gases in Deuterated Solvents Relevant to the Organometallic Chemist. *Organometallics* **2010**, *29*, 2176–2179.
34. Balci, M. *Basic 1H-and 13C-NMR Spectroscopy*; Elsevier B.V., Amsterdam, The Netherlands, 2005; p. 419.
35. Myllyoja, J.; Lindblad, M.; Käldström, M.; Piilola, R.; Ikonen, E. Renewable Hydrocarbons, Method for Producing the Same and the Use Thereof. EP3187482A1, 29.12.2015.
36. Minachev, K.M.; Shuikin, N.I.; Rozhdestvenskaya, I.D. Hydrogenation and dehydrogenation of hydrocarbons in presence of ruthenium and rhodium catalysts of low metal content. *Bull. Acad. Sci. Ussr Div. Chem. Sci.* **1954**, *3*, 277–281.
37. Pirogova, G.N.; Rimar', N.N.; Kalinina, G.E. Synergistic effect for bimetallic Ru-Tc catalysts of cyclohexane dehydrogenation. *Russ. Chem. Bull.* **1996**, *45*, 1857–1861.
38. Brunauer, S.; Emmett, P.H.; Teller, E. Adsorption of Gases in Multimolecular Layers. *J. Am. Chem. Soc.* **1938**, *60*, 309–319.
39. Barrett, E.P.; Joyner, L.G.; Halenda, P.P. The Determination of Pore Volume and Area Distributions in Porous Substances. I. Computations from Nitrogen Isotherms. *J. Am. Chem. Soc.* **1951**, *73*, 373–380.
40. Shen, X.; Garces, L.; Ding, Y.; Laubernds, K.; Zerger, R.P.; Aindow, M.; Neth, E.J.; Suib, S.L. Behavior of H2 chemisorption on Ru / TiO2 surface and its application in evaluation of Ru particle sizes compared with TEM and XRD analyses. *Appl. Catal. A Gen.* **2008**, *335*, 187–195.
41. Bergeret, G.; Gallezot, P. Particle Size and Dispersion Measurements. In *Handbook of Heteregeneous Catalysis*; Ertl, G., Knözinger, H., Schuth, F., Weitkamp, J., Eds.; WILEY-VHC Verlag GmbH & Co. KGaA: Weinheim, Germany, 2008; pp. 738–746, ISBN 978-3-527-31241-2.
42. Guerrero, H.; Lafuente, C.; Royo, F.; Lomba, L.; Giner, B. P P T behavior of several chemicals from biomass. *Energy Fuels* **2011**, *25*, 3009–3013.
43. Scanlon, James, T.; Willis, D.E. Calculation of Flame Ionization Detector Relative Response Factors Using the Effective Carbon Number Concept. *J. Chromatogr. Sci.* **1985**, *23*, 333–340.
44. Fogler, H.S. *Elements of Chemical Reaction Engineering*, 4th ed.; Pearson Education, Inc.: Westford, Massachusetts, MA, USA, 2006; pp. 66–67, ISBN 0-13-127839-8.
45. Kapteijn, F.; Gascon, J.; Nijhuis, T.A. Catalytic Reaction Engineering. In *Catalysis An Integrated Textbook for Students*; Hanefeld, U., Lefferts, L., Eds.; Wiley-VCH Verlag GmbH & Co.: Weinheim, Germany, 2008; pp. 221–271, ISBN 978-3-527-34159-7.
46. Boudart, M. Turnover Rates in Heterogeneous Catalysis. *Chem. Rev.* **1995**, *95*, 661–666.
47. Deutschmann, O.; Knözinger, H.; Kochloefl, K.; Turek, T. Heterogeneous Catalysis and Solid Catalysts, 1. Fundamentals. In *Ullmann's Encyclopedia of Industrial Chemistry*; Wiley-VCH Verlag GmbH & Co. KGaA: Weinheim, Germany, 2011; pp. 565–582, ISBN 9783527306732.